A Sliding Mode Voltage Controller and a Lyapunov-Based Current Controller for a Bridgeless Boost PFC

S. Yari-Alghar, S. Sarmad

Abstract-- In this paper, a bridgeless boost PFC (BBPFC) with a 2nd order sliding mode controller (SMC) as a voltage controller and a Lyapunov-based current controller is proposed. Using a bridgeless structure leads to less power dissipation due to the elimination of the diode bridge. Moreover, since the boost inductor operates as EMI filter, as well, the implementation costs and difficulties will decrease. On the other hand, a second order SMC is used to attenuate the voltage ripples and chattering. Since the voltage loop has no direct influence on the switching signal, the chattering problem will be mitigated significantly and high-frequency ripples will not appear in the gate signal of the converter. In addition, by using a Lyapunov-based current controller, the stability of the current controller is guaranteed. The experimental prototype of the system is provided. Experimental results show that BBPFC with SMC and Lyapunov-based controllers gives satisfactory results in improving the power quality of the input current.

Keywords: Bridgeless Structure, Lyapunov Controller, Power Factor Correction, Sliding Mode Controller.

I. INTRODUCTION

TRADITIONAL AC/DC converters mainly consist of an Electromagnetic Interference (EMI) filter, a diode bridge rectifier, and a smoothing capacitor. The most dominant drawbacks of these types of converters are current harmonics and reactive power they inject to the grid. Especially in medium and high-power applications, these two problems might cause detrimental effects to the grid. Therefore, it is mandatory to attenuate these harmful effects. One way to prevent current harmonics and reactive power to be injected to the grid is power factor correction (PFC) [1-4].

In [5], three major configurations and their derivatives for PFC application are surveyed. According to [5], boost converter is suitable for applications in which the output voltage needs to be higher than the input voltage (e.g., EV chargers). Several researches have been performed in order to improve boost PFC operation. In [6], a 100Hz switching scheme has been proposed for boost PFC to mitigate di/dt and dv/dt. As a result, slow-recovery diodes could be used. In [7], a feedforward control method is proposed for boost PFC that can reduce input current harmonic distortion, especially for applications in which the current loop crossover frequency is relatively low compared to the line frequency. This control method is claimed to be more effective than the existing feedback and feedforward control methods. In [8], a predictive current control method is proposed that can operate properly in both discontinuous (DCM) and continuous current (CCM) modes which results into higher efficiency and lower current distortion. In [9], a digital control scheme is addressed for boost PFC converter that operates in DCM. It is shown that this converter can fully compensate the current harmonics and reactive power of the rectifier. In [10], a control scheme based on duty ratio feedforward is proposed. This control scheme is claimed to work properly especially in zero crossing intervals. In [11], a predictive digital control is proposed so that the duty cycle needed for boost PFC switch for next half period is calculated. In addition, a feedforward component of input voltage is utilized in the control system; Hence, the output voltage is insensitive to the input voltage distortion.

In order to reduce input and output current ripple and the size of EMI filter, interleaved boost converters are utilized. An interleaved boost converter consists of two switches that operate with 180 phase difference [12,13]. In [14], a sliding mode digital control is proposed for an interleaved boost PFC. This control scheme leads to a constant switching frequency for interleaved boost PFC. Besides, the third harmonic is mitigated because of the proportionality between the input voltage and the average input current. In [15], a non-linear observer is designed so that there is no need to measure the boost inductor current anymore. Therefore, not only will the costs be declined, but also the noises during measurement will be avoided. In [16] a non-linear controller based on Lyapunov theory is provided for an interleaved boost PFC. This controller showed a robust performance under heavy disturbance situations. Moreover, since the control scheme is designed in the discrete domain, understanding the operation of the controller is simple.

Sliding mode controller (SMC) is a popular controller in performance under uncertain circumstances. However, in order to keep the desired parameter on zero, the switching frequency will be variable and thus, chattering will happen. The variable switching frequency can cause some problems in

S. Yari-Alghar a PhD student at Department of Electrical Engineering, Iran university of science and technology, Tehran, Iran (e-mail: sajjady1394@gmail.com).
S. Sarmad is with the R&D Department of Nian Electronic Co., Mashhad, Iran (e-mail: so.sarmad@gmail.com).

power electronic devices [17]. SMC is especially used in systems with uncertainties. In [18] a SMC is used in the control system of an double fed induction generator (DFIG). Since this controller has adaptive gains, uncertainties bounds are not important. Moreover, implementation of this system is possible due to the simplicity of the controller. On the other hand, [19] performs a comparison between the operation pf SMC and terminal SMC to control the output voltage of a cascade DFIG and in addition, robustness of two controllers is also examined. In [20], a SMC combined with artificial neural network (ANN) is presented to gain the advantages of two controllers. Using an improved PWM technique along with SMC-ANN led to more accuracy and robustness of the system. SMC controller is used to improve the operation of a shunt active power filter in [21]. The authors in [21] investigated an improved SMC which is based on state space average modelling which resulted in fast response of the controller and suitable compensation of shunt active power filter. In [22], a SMC is used as current controller in a buck-boost converter. By using this controller, a fast dynamic response, robustness, and stability is achieved. [23] proposes a novel maximum power point tracking (MPPT) algorithm for PV system. This SMC-based MPPT algorithm is applied to three different DC-DC converters and the results are compared.

In [24], a 2nd order SMC is proposed this SM controller is used to track the reference current in an active power filter. According to [24], this SM controller not only results fast dynamic response, but also ensures the stability of the system. Besides, due to the non-linearity characteristic of this controller, it can be used in non-linear systems such as bridgeless boost PFC. Some other factors that make this SMC a proper choice are simplicity in design and implementation, natural anti-wind up characteristics and inherent adaptively set coefficients.

In this paper, a Bridgeless Boost PFC (BBPFC) is used as an AC/DC device. The voltage controller is chosen to be the proposed 2nd order SMC in [24] that results in high robustness and stability. The SMC controller produces the reference peak of the input current. Subsequently, the proposed non-linear controller in [16] is used to track the reference current. The main contributions of this paper are:

(1) A bridgeless structure is used and therefore, the power dissipation can be reduced significantly since the diode bridge has been eliminated.

(2) By using a bridgeless converter, diode bridge and EMI filter will be eliminated and therefore, the implementation costs will be reduced. It is worth mentioning that the boost inductor in BBPFC can also operate as an EMI filter and therefore, there would be no need to extra inductor. While in some structures such as boost PFC (with diode bridge) or interleaved structures, an extra EMI filter is used.

(3) A robust 2nd order SMC is used that leads to improved stability in voltage control loop. In addition, since the SMC controller is used in the outer loop, chattering phenomenon causes less damage since SMC is not generating the control signal directly.

(4) The current controller is based on Lyapunov theorem and thus, it can ensure robustness and stability of the current control loop.

II. Configuration Of The System

Fig.1 shows the configuration of a BBPFC. It can be seen that the diode bridge has been eliminated. $V_{in}(t)$ is the voltage source which has the peak value of V_m. Inductor L is not only the boost inductor, but also acts like an EMI filter. I_{in} is input current which is to be in-phase with the source voltage. Q_1 and Q_2 are power mosfets and D_1 and D_2 are power diodes. In the next section it will be shown that Q_1 and D_1 with L form a boost converter in one half-cycle of the input voltage and subsequently, and with form another boost converter in the other half-cycle. Furthermore, is output capacitor, is the load, and is output voltage.

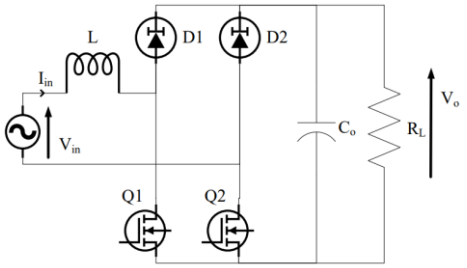

Fig. 1. Block diagram of a BBPFC

III. State Space Model Of The Bridgeless Boost Converter

In this section the state space modeling of the boost converter will be expressed. Fig.2 shows the current path of the BBPFC in each operation area. In the first half-cycle of input voltage (Fig.2 a), when Q_1 is ON, L is charging through Q_1 and reverse diode of Q_2. When Q_1 goes OFF, just similar to a casual boost converter, D_1 starts conducting and charges C_o. Fig.2 (a) indicates this operation. The blue arrows show the current path of the voltage source which are valid regardless of the state of Q_1. The green arrows are current path when Q_1 is ON and the yellow arrows represent the current path when D_1 conducts.

In the next half-cycle, when Q_2 is ON and L is charging through Q_2 and reverse diode of Q_1. Similar to the first half-cycle, when Q_2 goes OFF D_2 begins conducting and charges C_o. Fig.2 (b) expresses this process. The blue arrows show the current path of the voltage source which are valid regardless of the state of Q_2. The green arrows are current path when Q_2 is ON and the yellow arrows represent the current path when D_2 conducts.

Hence, it can be observed that the bridgeless converter

actually consists of two sets of boost converters, each operating at one half-cycle of the input voltage. Thus, the state space model of a bridgeless converter can be stated as a normal boost which is valid for a boost converter in each half-cycle. The state space equations for a boost converter are:

$$\frac{di_L}{dt}=\frac{1}{L}V_{in}-\frac{1-d}{L}V_c \tag{1}$$

$$\frac{dV_c}{dt}=\frac{1-d}{C}i_L-\frac{1}{RC}V_c \tag{2}$$

In Eq.1 and Eq.(2), i_L is inductor current, V_c is output capacitor voltage, V_{in} is input voltage, L, C_o, and R_L are inductor, capacitor and the load values, respectively, and d is the duty cycle of the power switch.

$$\begin{pmatrix} i_L(k+1) \\ V_c(k+1) \end{pmatrix}=\begin{pmatrix} a_{11} & a_{12} \\ a_{21} & a_{22} \end{pmatrix}.\begin{pmatrix} 1 & 0 \\ 0 & 1 \end{pmatrix} +\begin{pmatrix} 1 & 0 \\ 0 & 1 \end{pmatrix}.\begin{pmatrix} 1 & 0 \\ 0 & 1 \end{pmatrix}.d(k)+\begin{pmatrix} 1 & 0 \\ 0 & 1 \end{pmatrix}V_{in}(k) \tag{3}$$

IV. Control Scheme For BBPFC

The In [16], a digital control scheme for an interleaved boost PFC has been proposed. This control scheme firstly expresses the digital state space model of interleaved boost PFC using bilinear Tustin discretization method. Then, a Lyapunov energy function is defined to achieve the proper duty cycle for power switches. In addition, another Lyapunov function has been defined in terms of the integral of the error of the output capacitor voltage and input inductor current to minimize the errors even more. Since this control approach led to suitable results, it has been modified for a BBPFC. However, due to the elimination of the diode bridge and lesser number of passive elements, this configuration can be used in more power levels than the interleaved boost converter.

According to [16], using bilinear Tustin discretization method, the derivative of a variable in continuous domain can be expressed in discrete domain as [16]:

$$\frac{dx}{dt}=\frac{x(k+1)-x(k)}{T_s} \tag{4}$$

Using Eq. (4), state space equations stated in Eq. (1) and (2) for the bridgeless converter can be re-written as [16]:

$$i_L(k+1)=i_L(k)+\frac{T_s}{L}V_{in}(k)-\frac{T_s}{L}(1-d)V_c(k) \tag{5}$$

$$V_c(k+1)=\frac{T_s}{C}(1-d)i_L(k)+(1-\frac{T_s}{R_LC})V_c(k) \tag{6}$$

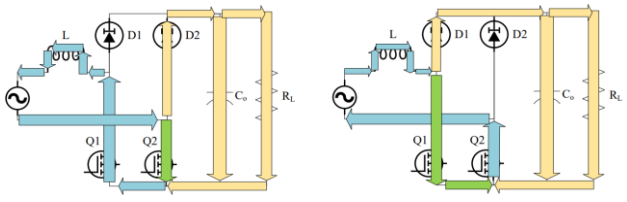

Fig. 2. Analysis of the current paths of the BBPFC

Converting Eq. (5) and (6) into matrix form results in [16]:

$$\begin{bmatrix} i_L(k+1) \\ V_c(k+1) \end{bmatrix}=\begin{bmatrix} 1 & -\frac{T_s}{L} \\ \frac{T_s}{C} & 1-\frac{T_s}{R_LC} \end{bmatrix}.\begin{bmatrix} i_L(k) \\ V_c(k) \end{bmatrix} +\begin{bmatrix} 0 & \frac{T_s}{L} \\ -\frac{T_s}{C} & 0 \end{bmatrix}\begin{bmatrix} i_L(k) \\ V_c(k) \end{bmatrix}d(k)+\begin{bmatrix} \frac{T_s}{L} \\ 0 \end{bmatrix}V_{in}(k) \tag{7}$$

According to [16], it is worthwhile to define two more state variables to mitigate the steady state error furthermore. These two variables are defined as the integral of the voltage and current error:

$$x_1=\frac{1}{K_{ii}}\int_0^t (i_L(k)-i_L^*(k))\,d\tau \tag{8}$$

$$x_2=\frac{1}{K_{iv}}\int_0^t (V_c(k)-V_c^*(k))\,d\tau \tag{9}$$

Converting Eq. (8) and (9) to discrete form results in [16]:

$$x_1(k+1)=x_1(k)+\frac{T_s}{K_{ii}}i_L(k)-\frac{T_s}{K_{ii}}i^*_L(k) \tag{10}$$

$$x_2(k+1)=x_2(k)+\frac{T_s}{K_{iv}}V_c(k)-\frac{T_s}{K_{iv}}V_c^*(k) \tag{11}$$

Combining Eq. (7) and the matrix form of Eq. (10) and (11) gives [16]:

$$\begin{bmatrix} i_L(k+1) \\ V_c(k+1) \\ x_1(k+1) \\ x_2(k+1) \end{bmatrix}=\begin{bmatrix} 1 & -\frac{T_s}{L} & 0 & 0 \\ \frac{T_s}{C} & 1-\frac{T_s}{R_LC} & 0 & 0 \\ \frac{T_s}{K_{ii}} & 0 & 1 & 0 \\ 0 & \frac{T_s}{K_{ii}} & 0 & 1 \end{bmatrix}.\begin{bmatrix} i_L(k) \\ V_c(k) \\ x_1(k) \\ x_2(k) \end{bmatrix}+\begin{bmatrix} \frac{T_s}{L} \\ 0 \\ 0 \\ 0 \end{bmatrix}v_{in}(k)+ \begin{bmatrix} 0 & \frac{T_s}{L} & 0 & 0 \\ -\frac{T_s}{C} & 0 & 0 & 0 \\ 0 & 0 & 0 & 0 \\ 0 & 0 & 0 & 0 \end{bmatrix}.\begin{bmatrix} i_L(k) \\ V_c(k) \\ x_1(k) \\ x_2(k) \end{bmatrix}d(k)+\begin{bmatrix} 0 \\ 0 \\ -\frac{T_s}{K_{ii}} \\ 0 \end{bmatrix}i_L^*(k)+\begin{bmatrix} 0 \\ 0 \\ 0 \\ -\frac{T_s}{K_{iv}} \end{bmatrix}V_c^*(k) \tag{12}$$

Eq. (12) indicates the final discrete state space model of a bridgeless boost converter. In order to minimize the tracking error of the voltage and current, an energy function is defined as [16]:

$$V=\frac{1}{2}[i_L(k+1)-i_L^*(k+1)]^2+\frac{1}{2}[V_C(k+1)-V_C^*(k+1)]^2 \tag{13}$$

To find the optimum duty cycle for the bridgeless converter, the derivative of the energy function V with respect to $d(k)$ is calculated as [16]:

$$\frac{\partial V}{\partial d(k)}=0 \tag{14}$$

Therefore, $d(k)$ can be achieved as:

$$d(k) = -\frac{\frac{T_s}{L}V_C(k)\gamma_1 - \frac{T_s}{C}i_L(k)\lambda_1}{[\frac{T_s}{L}V_C(k)]^2 + [\frac{T_s}{C}i_L(k)]^2} \quad (15)$$

where:

$$\gamma_1 = i_L(k) - \frac{T_s}{L}V_C(k) - \frac{T_s}{L}V_{in}(k) - i_L^*(k+1) \quad (16)$$

$$\lambda_1 = \frac{T_s}{C}i_L(k) + (1 - \frac{T_s}{R_L C})V_C(k) - V_C^*(k+1) \quad (17)$$

As stated before, the two extra state variables are defined to ensure the least steady state error of the capacitor voltage and inductor current. To achieve this goal, another energy function, V_{cor}, is defined as [16]:

$$V_{cor} = \frac{1}{2}L\, x_1(k+1)^2 + \frac{1}{2}C\, x_2(k+1)^2 \quad (18)$$

To find the optimum duty ratio, the derivative of V_{cor} with respect to $d(k-1)$ is calculated as [16]:

$$\frac{\partial V_{cor}}{\partial d(k-1)} = 0 \quad (19)$$

Therefore, d_{cor} can be derived using Eq. (19) as:

$$d_{cor}(k-1) = \frac{CV_C(k-1)\gamma_2 - Li_L(k-1)\lambda_2}{\frac{CT_s^2}{LK_{ii}}V_C^2(k-1) + \frac{LT_s^2}{CK_{iv}}i_L^2(k-1)} \quad (20)$$

where:

$$\gamma_2 = x_1(k) + \frac{T_s}{K_{ii}}\left\{i_L(k-1) - i_L^*(k) + \frac{T_s}{L}V_{in}(k-1) - \frac{T_s}{L}V_C(k-1)\right\} \quad (21)$$

$$\lambda_2 = x_2(k) - \frac{T_s}{K_{iv}}V_C^*(k) + \frac{T_s}{K_{iv}}\left\{\frac{T_s}{C}i_L(k-1) + (1 - \frac{T_s}{R_L C})V_C(k-1)\right\} \quad (22)$$

Eventually, the duty cycle of the power switch can be calculated as [16]:

$$d_{eff}(k) = d(k) + d_{cor}(k-1) \quad (23)$$

This duty cycle should be applied to Q_1 in the first half-cycle of the input voltage and to Q_2 during the second half-cycle.

V. Reference Current Generator

In order to generate the reference current, an SMC proposed in [24] is used in this paper to generate the reference current. The input to the SM controller is the output voltage error. which is considered as the sliding surface [24]:

$$\sigma = V_{oref} - V_o \quad (24)$$

where V_o is the output voltage and V_{oref} is the reference output voltage. As mentioned in [24], the control law should be selected so that both the error, σ , and its derivative, $\dot{\sigma}$, reach zero value. To achieve this, the super-twisting control law is used. The super-twisting controller acts like an adaptive PI controller. Hence, it consists of two parts, a proportional part (U_1, Eq. (25)) and an integrator part (U_2, Eq. (26)) [24].

$$U_1 = K_p\sqrt{|\sigma|}\, sign(\sigma) \quad (25)$$

$$U_2 = \begin{cases} \int K_i\, sign(\sigma)\, dt & |U| < U_{\max} \\ -\int U\, dt & |U| > U_{\max} \end{cases} \quad (26)$$

In Eq. (26), U is the total control law which can be obtained as [24]:

$$U = U_1 + U_2 \quad (27)$$

With regard to Eq. (26), it can be observed that this SM controller has an anti-winding property and thus, avoids the control signal to saturate [24].

The output signal of the SM controller, U , is actually the peak value of the reference current, I_m^* .Therefore, it is essential to generate a sinusoidal wave in-phase with the input voltage. The production of I_m^* with the generated sine wave, the reference current waveshape would be achieved. To be more precise:

$$I_{ref} = I_m^* \sin(\omega t) \quad (28)$$

In order to generate the sine wave, samples are taken from the input voltage ($V_{in}(t)$). These samples are then multiplied by a gain to reduce the amplitude of the sine wave. This gain is $1/V_m$ where V_m is the peak value of the input voltage. It is worth noticing that even though the real amplitude of the input voltage may change, by considering the standard amount of change in the amplitude (5%) the error would be negligible. Hence, using Eq. (28), I_{ref} can be generated. Fig.3 indicates the overall block diagram of the BBPFC.

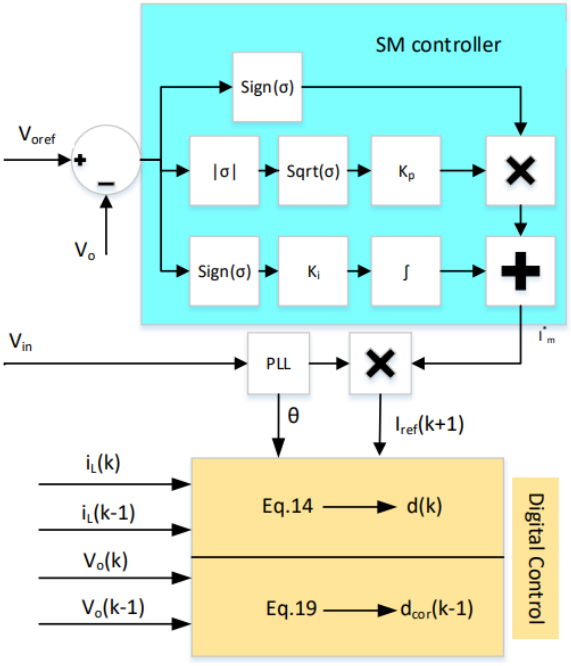

Fig. 3. Overall Block Diagram of the BBPFC

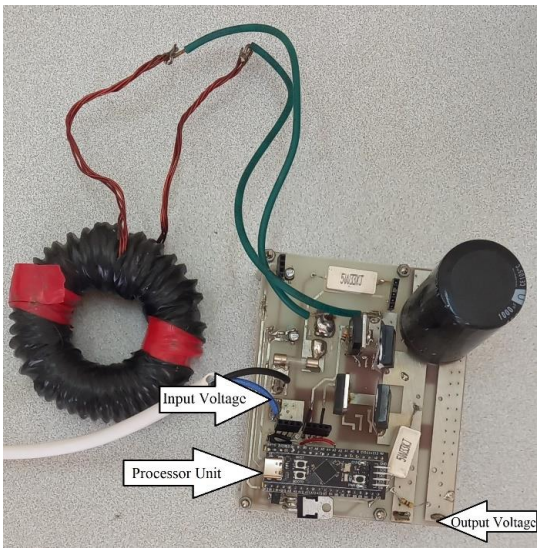

Fig. 4. Experimental Prototype

TABLE I
SYSTEM PARAMETERS

V_m	85	V
V_{oref}	130	V
L	330	µH
C_o	2	mF
R_L	200 140 70	Ω
Current sensor gain	40	mV/A

VI. EXPERIMENTAL RESULTS

In this section, the experimental results of the operation of the BBPFC with proposed SMC controller for the voltage loop and digital Lyapunov-based controller for the current loop are proposed. Fig.4 shows the prototype used in this experiment. Considering the configuration in Fig.1, the parameters of the system are as Table.1 It is worth mentioning that the current sensor used in this prototype is ACS758 which according to the datasheet, it has a gain of 40mV/A. In addition, the waveshapes of the input voltage and current are measured from the sensors and thus, the numbers in the figures of the voltage and current should be divided by the sensors' gains. Fig.5 depicts the waveshape of the input voltage (the blue wave) and the input current (the yellow wave). The load is set at 200Ω in this circumstance. It can be seen that not only is the current in-phase with the input voltage, but also has a similar shape to a sinusoidal compared to a regular diode bridge rectifier.

Fig.6 shows the input voltage and current waveshapes with a 140Ω load. It can be observed that with higher load, the BBPFC operates better and current regulation has been achieved properly. Additionally, the current is in-phase with the input voltage which results into less reactive power in the line. Fig.7 shows the operation of the BBPFC with the heaviest load, 70Ω. Similar to the previous loads, the current has a lesser THD compared to the diode bridge current and besides, it is in-phase with the input voltage.

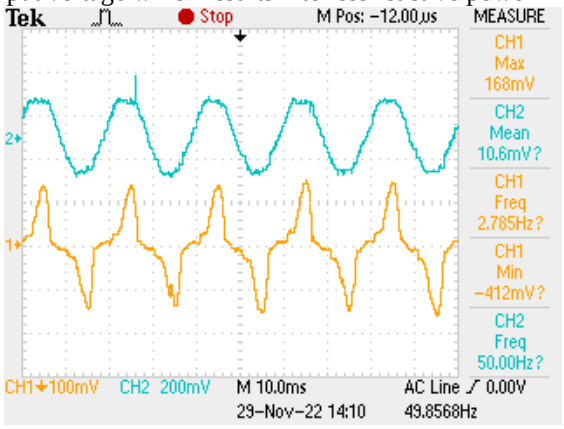

Fig. 5. Voltage and Current Waveshapes for 200Ω load

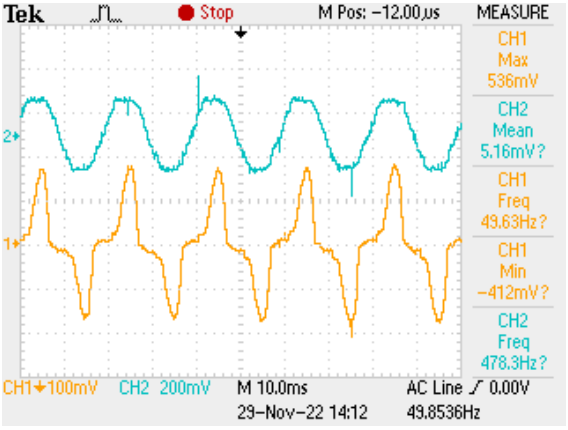

Fig. 6. Voltage and Current Waveshapes for 140Ω load

VII. CONCLUSION

In this paper, new voltage and current controllers for a bridgeless boost PFC -BBPFC- were proposed. BBPFCs usually have two control loops. The voltage controller is a 2nd order sliding mode controller -SMC- and the current controller is a digital controller based on Lyapunov theorem. Additionally, the bridgeless structure used in this paper leads to less power dissipation since there is no diode bridge and thus, this converter can operate in higher power range. An experimental prototype of this converter is also provided with STM32F103C8T6 processor. This microcontroller is cheap and therefore, the implementation costs will reduce. The results from the experimental prototype show a satisfactory performance of the BBPFC with proposed voltage and current controllers. To be more precise, the current waveshape is much closer to the desired sinusoidal shape compared to the conventional diode bridge rectifier. Moreover, the current is in-phase with the input voltage which leads to reactive power compensation.

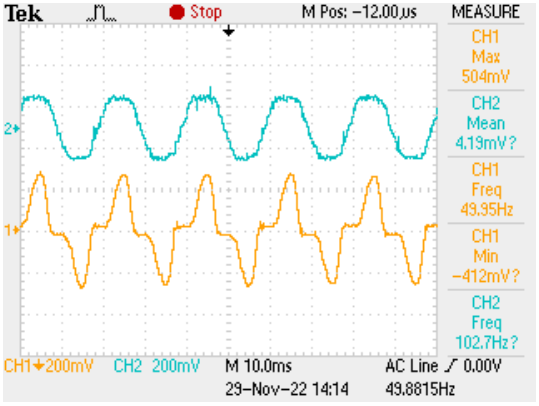

Fig. 7. Voltage and Current Waveshapes for 70Ω load

VIII. REFERENCES

[1] I.U. Kim, B.K. Bae, and J.W. Choi, "New control strategy for interleaved PFC rectifiers using Lyapunov function," *Journal of Power Electronics*, vol. 21, no. 2, pp. 464-474, 2021.

[2] J. Dadkhah, C. N. M. Ho, J. X. Liu, Y. Xu, "Comprehensive study and performance evaluation of an interleaved gan-based pfc with magnetic component size reduction." *IEEE Transactions on Industrial Electronics*, vol. 71, no. 11, pp. 14075-14085, 2024.

[3] H. J. Seon, H. G. Koh, and Y. J. Choi, "Asymmetric Phase MPCC Interleaving Method for Boost PFC Converter With Enhanced Input Current Harmonic Characteristic." *IEEE Access*. Vol. 13, pp. 9955-9964, 2025.

[4] S. Saha, and S. K. Singh, "Restricted interleaving phenomenon in Interleaved Boost PFC with leg sharing APF circuit." *IEEE Transactions on Industry Applications*. Vol. 60, no. 6, pp. 8963-8975, 2024.

[5] S. S. Sayed and A. M. Massoud, "Review on State-of-the-Art Unidirectional Non-Isolated Power Factor Correction Converters for Short-/Long-Distance Electric Vehicles," *IEEE Access*, vol. 10, pp. 11308-11340, 2022.

[6] L. Rossetto, G. Spiazzi and P. Tenti, "Boost PFC with 100-Hz switching frequency providing output voltage stabilization and compliance with EMC standards," *IEEE Transactions on Industry Applications*, vol. 36, no. 1, pp. 188-193, 2000.

[7] M. Chen and Jian Sun, "Feedforward current control of boost single-phase PFC converters," *IEEE Transactions on Power Electronics*, vol. 21, no. 2, pp. 338-345, 2006.

[8] F. Z. Chen and D. Maksimović, "Digital Control for Improved Efficiency and Reduced Harmonic Distortion Over Wide Load Range in Boost PFC Rectifiers," *IEEE Transactions on Power Electronics*, vol. 25, no. 10, pp. 2683-2692, 2010.

[9] Z. Z. Ye and M. M. Jovanovic, "Implementation and performance evaluation of DSP-based control for constant-frequency discontinuous-conduction-mode boost PFC front end," *IEEE Transactions on Industrial Electronics*, vol. 52, no. 1, pp. 98-107, 2005.

[10] D. M. Van de Sype, Koen De Gusseme, A. P. M. Van den Bossche and J. A. Melkebeek, "Duty-ratio feedforward for digitally controlled boost PFC converters," *IEEE Transactions on Industrial Electronics*, vol. 52, no. 1, pp. 108-115, 2005.

[11] Wanfeng Zhang, Guang Feng, Yan-Fei Liu and Bin Wu, "A digital power factor correction (PFC) control strategy optimized for DSP," *IEEE Transactions on Power Electronics*, vol. 19, no. 6, pp. 1474-1485, 2004.

[12] L. Huber, B. T. Irving and M. M. Jovanovic, "Open-Loop Control Methods for Interleaved DCM/CCM Boundary Boost PFC Converters," *IEEE Transactions on Power Electronics*, vol. 23, no. 4, pp. 1649-1657, 2008

[13] A. V. J. S. Praneeth and S. S. Williamson, "A Review of Front End AC-DC Topologies in Universal Battery Charger for Electric Transportation," in *Proc. 2018 IEEE Transportation Electrification Conference and Expo (ITEC)*, Long Beach, CA, USA, pp. 293-298.

[14] A. Marcos-Pastor, E. Vidal-Idiarte, A. Cid-Pastor and L. Martinez-Salamero, "Interleaved Digital Power Factor Correction Based on the Sliding-Mode Approach," *IEEE Transactions on Power Electronics*, vol. 31, no. 6, pp. 4641-4653, 2016.

[15] M. Pahlevani, S. Pan, S. Eren, A. Bakhshai and P. Jain, "An Adaptive Nonlinear Current Observer for Boost PFC AC/DC Converters," *IEEE Transactions on Industrial Electronics*, vol. 61, no. 12, pp. 6720-6729, 2014.

[16] P. Das, M. Pahlevaninezhad, J. Drobnik, G. Moschopoulos and P. K. Jain, "A Nonlinear Controller Based on a Discrete Energy Function for an AC/DC Boost PFC Converter," *IEEE Transactions on Power Electronics*, vol. 28, no. 12, pp. 5458-5476, 2013.

[17] A. Levant, "Principles of 2-sliding mode design," *Automatica*, vol. 43, no. 4, pp. 576-586, 2007.

[18] M. Ehsani, A. Oraee, B. Abdi, V. Behnamgol, and S. M. Hakimi, "Adaptive Dynamic Sliding Mode Algorithm for BDFIG Control," *Iranian Journal of Electrical & Electronic Engineering*, vol. 19, no. 1, 2405, 2023.

[19] H. Zahedi Abdolhadi, G. Arab Markadeh, and S. Taghipour Boroujeni, "Sliding Mode and Terminal Sliding Mode Control of Cascaded Doubly Fed Induction Generator," *Iranian Journal of Electrical & Electronic Engineering*, vol. 17, no. 3, p1, 2021.

[20] H. Benbouhenni, "Sliding Mode with Neural Network Regulator for DFIG Using Two-Level NPWM Strategy," *Iranian Journal of Electrical & Electronic Engineering*, vol. 15, no. 3, pp. 411-419, 2019.

[21] A. Zakipour, K. Aminzare, and M. Salimi, "Sliding Mode Controller Design for Stabilization of the Three-Phase Grid-Connected Inverters in the Presence of Unbalanced Local Loads," *Iranian Journal of Electrical & Electronic Engineering*, vol. 18, no. 3, 2125, 2022.

[22] A. Safari and H. Ardi, "Sliding Mode Control of a Bidirectional Buck/Boost DC-DC Converter with Constant Switching Frequency," *Iranian Journal of Electrical & Electronic Engineering*, vol. 14, no. 1, pp. 69-84, 2018.

[23] J. Ghazanfari and M. Maghfoori Farsangi, "Maximum Power Point Tracking Using Sliding Mode Control for Photovoltaic Array," *Iranian Journal of Electrical & Electronic Engineering*, vol. 9, no. 3, pp. 189-196, 2013.

[24] C. Gong, W. K. Sou and C. S. Lam, "Second-order sliding-mode current controller for LC-coupling hybrid active power filter." *IEEE Transactions on Industrial Electronics*, vol. 68, no. (3), pp. 1883-1894, 2020.

IX. BIOGRAPHIES

Sajjad Yari-Alghar is currently PhD student at Iran University of Science and Technology. He was graduated from IUST in power electronics major and his research interests are power electronic converters, converter control, non-linear control application in power electronics, etc.

Soroush Sarmad received B.S. degree in electrical engineering and M.S. degree in power electronics in Faculty of electrical and computer engineering, University of Birjand in 2021, and 2023.
He is currently working as Research and Development Engineer in related power electronic company, Nian Electronic Co. Mashhad, Iran.
His research interests include digital control and nonlinear controller design of different power electronics converters, specially renewable energy, energy storage sytems, and power quality converters.